ORIGINAL

Flow Dynamics and Analyte Transfer in a Microfluidic Device for Spatial Two-Dimensional Separations

Noor Abdulhussain[1,2] · Raoul Fix[3] · Suhas Nawada[1,2] · Theodora Adamopoulou[1,2] · Peter Schoenmakers[1,2]

Abstract

In the last decade, chip-based separations have become a major area of interest in the field of separation science, especially for the development of "spatial" two-dimensional liquid chromatography (^{x}LC×^{x}LC). In ^{x}LC×^{x}LC, the analytes are first separated by migration to different positions in a first-dimension (^{1}D) channel and subsequently transferred with the aid of a flow distributor in a perpendicular direction to undergo a second-dimension (^{2}D) separation. In this study, several designs for ^{2}D separations are explored with the aid of computational fluid dynamics simulations. There were several aims of this work, viz. (1) to investigate the possible anomalies arising from the location of analyte bands in the first-dimension channel before transfer to the second dimension induced by the flow distributor, (2) to study the distribution ratio of the analytes across the different outlets of the ^{1}D channel, and (3) to study the flow behaviour confinement in the flow distributor. In all designs, the simulated absolute flow velocity was not equal in all regions of the ^{1}D channel. The extreme segments showed higher velocities compared to the central zones. This will eventually influence the migration times (first moments) and the variances (second moments), as confirmed by CFD results. The study has contributed to the understanding of the effects of the peak locations and, ultimately, to progress in spatial 2D-LC separations.

Keywords Two-dimensional spatial separation · Computational fluid dynamics · Multi-dimensional separation

Introduction

Comprehensive two-dimensional liquid chromatography (LC×LC) has become an established technique in many domains, such as food science, life science (metabolomics, proteomics), and polymer industry [1]. LC×LC provides more separation power and added chemical selectivity in comparison with one-dimensional (1D)-LC by the addition of the second dimension. Separation power for complex mixtures is best expressed in terms of peak capacity. LC×LC provides a possible increase in peak capacity by about an order of magnitude and a decrease in analysis time by about two orders of magnitude in comparison with high-resolution 1D-LC. Under certain conditions, notably, when using active-modulation techniques [2], LC×LC may also provide increased detection sensitivity. Column-based, "temporal" LC×LC methods are now well established and quite powerful, with commercial instruments available from several manufacturers. In such temporal systems, (many) fractions from the first-dimension effluent are successively separated in a fast second-dimension separation. To make full use of the attainable peak capacity in any kind of multi-dimensional LC system, it is essential that the selectivity in the different dimensions is vastly different. If the analysis time in one dimension is totally independent of that in another dimensions, we speak of orthogonal separations. Chromatographers also speak of a "degree of orthogonality" to describe the extent to which selectivities differ.

Chip-based separations are a major area of interest in separation science. Attempts have been made by several research groups to implement temporal two-dimensional separations in microfluidic devices [3–6]. Such an approach promises great reduction in the amounts of

✉ Noor Abdulhussain
   n.abdulhussain@uva.nl

1 Van't Hoff Institute for Molecular Sciences, Science Park, University of Amsterdam, 1098 HX Amsterdam, The Netherlands

2 The Centre for Analytical Sciences Amsterdam (CASA), University of Amsterdam, 1098 HX Amsterdam, The Netherlands

3 Physical Chemistry and Soft Matter, Wageningen University and Research, 6708 WE Wageningen, The Netherlands

solvents and sample needed. However, the separation performance and analysis times that can be obtained with such systems can only be compared with those obtained with column-based LC×LC systems if equally (ultra-) high pressures can be employed.

An alternative format is "spatial" LC×LC [7, 8]. In two-dimensional spatial LC×LC, the analytes are subsequently moved from their characteristic positions after the first-dimension ([1]D) separation in a perpendicular direction to undergo a second-dimension ([2]D) separation. In this [2]D direction, analytes are either moved to a new characteristic position in the two-dimensional plane ([x]LC×[x]LC) [9] or eluted from the [2]D region ([x]LC×[t]LC) [10, 11]. In a microfluidic format, an array of [2]D microchannels may be used to simultaneously separate analytes that are spatially separated in a [1]D channel. Using this approach there is no time for the [2]D separation, contrary to (column-based) temporal LC×LC, where the [2]D separation needs to be completed before the next fraction is collected (and, thus, needs to be very much faster than the first-dimensional). The sampling rates depend on the modulation times that are required. Shorter modulation times will result in more fractions being collected and transferred to the second dimension, thus decreasing the likelihood of undersampling of the 1D separation and/or reducing the total analysis time. In principle, the total attainable peak capacity is considerably improved for spatial LC×LC, while the analysis time can be shorter.

Another important consideration in spatial LC×LC is the efficient transfer of samples between the dimensions. This plays a critical role in achieving good separation performance. In a chip-based system with multiple [2]D channels, the uniformity of sample plugs transferred to each of the parallel second-dimension channels is a vital aspect. It is undesirable that different amounts of eluent and, therefore, different volumetric fractions of the separated sample after the [1]D separation are transferred to the different [2]D channels. In that case, if one analyte is distributed across more than one [2]D channel, it will show different migration times and bandwidths upon elution from each channel. In that case, one analyte may give rise to multiple peaks, unless the different detector traces from the different channels are corrected with advanced algorithms.

Also, another critical aspect of spatial chip-based systems is that the [1]D separation should be confined within its channel with little or no dispersion of analytes in other directions.

Isoelectric focusing (IEF) is an electro-driven separation technique, which relies on a voltage drop along the channel, rather than a pressure drop. Therefore, IEF becomes an interesting option for implementation as a.[1]D separation in a spatial LC×LC device. In principle, focusing analytes at specific points always favours resolution and detection sensitivity. The peak widths (standard deviation σ_f) can be controlled by varying the channel length (*L*) and the applied voltage (*V*) according to Refs. [12, 13]

$$\sigma_f = \frac{L}{\sqrt{V}}. \tag{1}$$

In a device with a limited number of second-dimension channels, rather than a continuous bed, there may be an optimum value of σ_f. Creating band widths in the first dimension that are much narrower than the distance between [2]D channels may be overkill. If the band widths are too large, analyte peaks will be distributed across multiple [2]D channels and the overall resolution and peak capacity will suffer. This implies that the length of this [1]D channel, which is normally not important for the resolution in IEF, will be important for spatial separations.

Also important is the optimization of the chip design, especially concerning sample transfer between the two separation domains. There are several published studies in which the sample transfer considering from a [1]D channel (e.g. IEF) to a series of parallel [2]D channels and a flat-bed structure is investigated [5, 9, 14]. Yang et al. developed a device with a zig-zag [1]D (IEF) channel to minimize sample tailing after transfer [9]. "Back-biasing" channels were incorporated outside the range of [2]D channels to achieve a more uniform sample transfer. Both the geometries of the [1]D channel and that of the inlets of the [2]D channels were found to affect sample transfer. A study from the same research group concerned the importance of an optimized chip design based on computational fluid dynamics (CFD) simulations [15]. The authors concluded that shifting the flow distributor (FD) by half the inter-channel distance, such that the [2]D channels are located between the exits of the flow distributor, led to a more efficient sample transfer than when the FD and [2]D channels were directly opposite.

The flow behaviour within a device may also influence the sample transfer between the two dimensions. Ideally, when closing the exits of the [1]D channel and switching on the flow from the FD, the velocity in the [1]D channel will become equal at all points. If this is not the case, the uneven flow velocities will affect the transfer of analyte bands and lower the overall efficiency of the [2]D separation.

In this study, we aim to explore possible designs for 2D-separation devices, with specific focus on an experimental and computational (CFD) study of the resulting band broadening. We aim to investigate the possible effect of diffusion if proteins are held in place in the [1]D channel before being eluted in a secondary direction using a flow distributor. We also aim to explore the recovery of protein analytes following migration in two different directions in a device with multiple parallel second-dimension separation channels. A final objective is to calculate the position

of analytes at the end of the ^{1}D step using elution data from a "blank" ^{2}D step (no stationary phase present).

Materials and Methods

Materials

The Formlabs durable resin (RS-F2-DUCL-02) was purchased from Formlabs (Berlin, Germany). 2-Propanol was obtained from Biosolve (Valkenswaard, The Netherlands). PME Natural Food Colours (red and green) were obtained from Knightsbridge PME (Enfield, UK). PEEK tubings (0.5 mm i.d., 1.6 mm o.d.) were purchased from VWR International (Amsterdam, The Netherlands). Norland Optical Adhesive 63 was purchased from Norland Products (Jamesburg, NJ, USA). The 2 mL glass vials were purchased from Sigma-Aldrich (Darmstadt, Germany).

Instrumentation

The 3D objects were fabricated through stereolithography (SLA) printers using a Form 3 + 3D printer (Formlabs). The peak parking measurements were performed on an Agilent Technologies 1100 series HPLC system (Agilent, Waldbronn, Germany). For the solvent delivery, LC pump Shimadzu prominence LC-20AD ('s Hertogenbosch, The Netherlands) was used.

Computational Fluid Dynamics (CFD)

For CFD simulations, ANSYS Workbench Fluid and Structures Academic package (versions 16.2–17.2) was used (ANSYS, Canonsburg, PA, USA). CFD is based on the fundamentals of Navier–Stokes equations, which describe the motion of viscous fluids with the conservation of momentum, mass, and energy [16]. All simulations were performed using the Fluent solver. All types of design studied were discretized in a similar manner with ANSYS Meshing. A 2D geometry was created for several devices. The 2D cross section was divided into the different parts of the geometry, viz. the flow distributor, ^{1}D channel, right and left outlets, and all the 2D outlets (see Fig. 1). The device consists of an inlet at the top with room for a #10–32 UNC fitting, a cylindrical ^{1}D channel with a length of 60.0 mm and internal diameter of 1.40 mm. The five outlets that represent the ^{2}D channels are placed with a distance of 13.5 mm and with a length of 10.0 mm and a diameter of 1.40 mm. The 2D design was then transferred to ANSYS Meshing, to create an unstructured triangular grid with fixed maximum cell size of 100 μm. All cases were solved for flow and species transport.
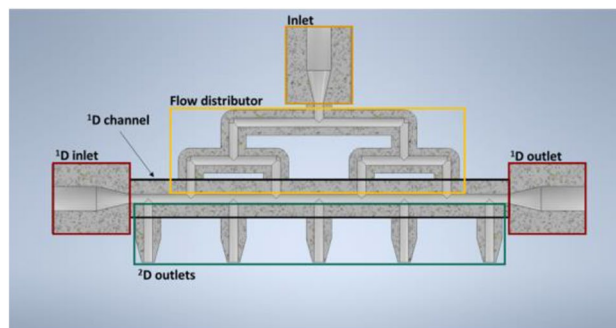

Fig. 1 Cross section of the device with five 2D outlets. **a** Top inlet is the flow distributor (orange box), **b** the ^{1}D channel (black box), **c** the right and left inlets connected to the ^{1}D channel (dark blue box), **d** the flow distributor (light blue box) and **e** the ^{2}D outlets (green box)

Steady-State Simulation for Velocity Profiles

A steady-state velocity profile was simulated with a flow applied from the flow distributor inlet (top in Fig. 1). The velocity at the inlet was set to 1 mm/s before the flow was divided across four inlets of the ^{1}D channel, to finally leave through five or nine outlets. In an ideal situation, the flow would be equally divided across the flow distributor and equal flow rates (in different directions) would be obtained throughout the ^{1}D channel. To investigate the velocities in the x- and y-directions in the ^{1}D channel, the calculated velocities at 100 evenly spaced points along a line through the middle of the ^{1}D channel ($y = 0$) were used. The channel was divided in imaginary segments, as indicated in Fig. 2c. The flow velocities in the x-direction were recorded at each of these points for each mesh size. The ends of the respective segments corresponded with an x-velocity of zero. These points should match the centres of the inlets and those of the outlets and all segment lengths should be equal.

Transient Simulations

Transient simulations were performed with tracer injections. The tracer species (with properties resembling proteins) were introduced in the device by using a custom field function, which created a normal distribution at a specified point. Courant–Friedrichs–Lewy (CFL) condition is satisfied. The time step was determined by the smallest element length divided by the maximum velocity. The smallest element length was calculated by taking the square root of the minimum cell volume. At every time step, the concentrations of the tracer were recorded at 10 mm and 5 mm distance from the outlets of the ^{2}D channels. This resulted in the profiles of the concentration of the tracer vs. time. For tracers split across multiple outlet channels, tracer concentrations were measured in several control lines. In processing the data, values smaller than 0.1% of the maximum value
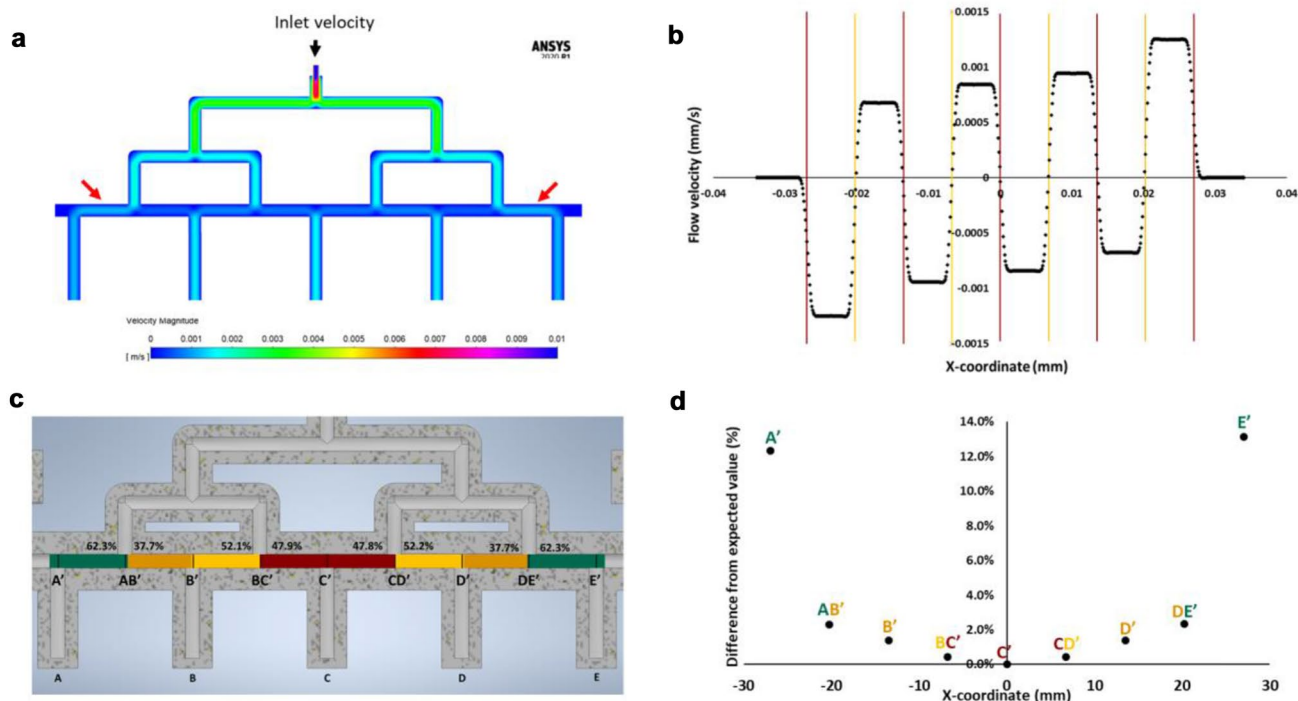
Fig. 2 Flow velocities calculated for a device with five outlets to ^{2}D channels. **a** colour plot of the flow velocities, **b** flow profile along the *x*-velocity in the ^{1}D channel with red and yellow lines highlighting the exits of the FD, **c** the various segments of the ^{1}D channel, with flow-inversion points indicated and the split ratio in percentage and **d** variations in the length of segments ending at the indicated position (letter code), relative to the expected values

were ignored (baseline). The tracer profiles were subjected to moment analysis (first and second moments). The basic prinicples of moment analysis are described in the supplementary material (S1).

3D Printing of the Devices

Microfluidic devices were designed using Autodesk Inventor (Autodesk, San Rafael, CA, USA) and SLA printed. The design was converted to STL format, loaded through the 3D-printer software interface (Formlabs), and printing orientation and settings were optimized. After 3D printing, devices were post-processed by sonication during about 1 h, followed by flushing of channels with 2-propanol and compressed air to remove any uncured resin in the channels. Finally, parts were placed in a Pico Flash UV chamber (type 87 DR-301C, 36 W, 365 nm; 3DXS, Erfurt, Germany) and cured for 60 min under UV light at a temperature of 60 °C. To make the devices connectable, the PEEK tubing was cut and secured with optical glue to the device.

Experimental Evaluation of Printed Devices

To study the effect of the flow profiles a device with five outlet was 3D printed. The inlet and outlet of the ^{1}D channel were closed with 10–32 blind nuts and the inlet of the flow distributor was connected to the pump. Small sections of PEEK tubing (0.5 mm i.d., 1.6 mm o.d., 8 mm length) were inserted into the outlets of the device to create a slightly increased backpressure. Also, 150-mm lengths of silicone tubing (3 mm i.d., 6 mm o.d.) were added to each outlet to transport the solvent to the collection vials. It is essential that the device is filled completely and that no air bubbles are present. Therefore, the device was clamped upside down in a vertical position, allowing easier removal of all air present in the device while it is being filled with water. Empty vials were weighed and placed underneath each ^{2}D outlet to collect the effluent. The device was then flushed with a solution of red dye in water at a flowrate of 4 ml/min for visualization. After 1 min, the flow was stopped and the vials were weighed. The mass percentage per outlet could be calculated from the total weight collected and compared with the results of the CFD simulations. This experiment was repeated five times.

Results and Discussion

Artefacts Induced by the Flow Distributor

The velocity profiles of the ^{2}D step was simulated to investigate the flow velocities at the outlets of the FD as described in "Computational fluid dynamics (CFD)". The inlet velocity was set at 0.01 mm s^{-1} for a target outlet velocity of 0.002 mm s^{-1}. Ideally, the flow should be equally divided across the five outlets of the flow distributor and the magnitude of the flow should be equal in each segment of the ^{1}D channel. An example of the calculated velocity profiles in FD is shown in Fig. 2a. Slight differences are observed in the magnitude of the velocity in different segments of the ^{1}D channel. At the extremes of the ^{1}D channel, higher velocities are observed (brighter colours, indicated by the red arrows in Fig. 2a). The x-velocity in the ^{1}D channel yields a profile as shown in Fig. 2b. Around the exits of the FD, the flow in the ^{1}D channel switches direction. Between the exits, the velocity is constant, as is evident from the plateaus in Fig. 2b. The absolute values of the velocities at the plateaus are significantly higher at the extremes of the design. This is desirable because the first and last ^{2}D channels are only fed from one direction. However, the higher velocities at the extremes of the ^{1}D channels do not compensate completely for this aspect of the design, as the absolute flow rates into the first and last outlet channels are still lower than the combined flow rates into the remaining channels. The various segments are indicated with different colours in Fig. 2c. The outer segments (dark green) show the highest absolute velocities in the ^{1}D channel at 1.25 mm s^{-1}, while the centre segments (dark red) show velocities of 0.84 mm s^{-1}. In the yellow segments, the velocity is 0.94 mm s^{-1}, while the lowest velocities (0.67 mm s^{-1}) are observed in the orange segments.

Ideally, all flow segment lengths are equal, i.e. segments B, C and D are of equal length. In practice, there are slight deviations in the location of the inversion points (boundaries between two segments). The inversion points are indicated by vertical lines in Fig. 2b, a letter code (letters plus prime) along the ^{1}D channel in Fig. 2c, and the labels of the points in Fig. 2d. The location of the inversion points deviates somewhat from the expected positions, corresponding with the various in- and outlets of the design. The relative deviations of the segment lengths are plotted against the design position. The outer left and outer right segments ending at A' and E', respectively, are 12.34% and 13.11% longer than expected. The inner segments (between AB' and DE') show deviations of less than 3%.

The variations in flow velocities and segment lengths are related. To reduce the variation in both, a device with
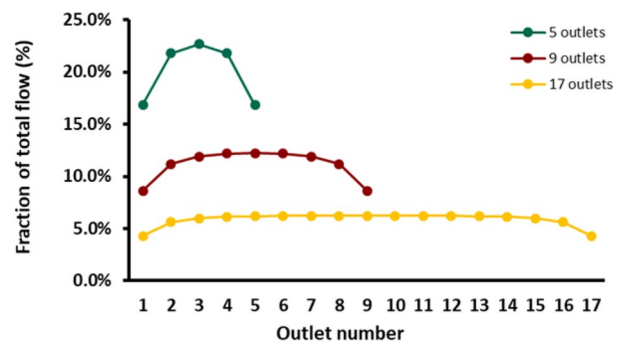

Fig. 3 Mass-average velocities through the different outlets of devices with 5 (green), 9 (dark red) and 17 (dark yellow) outlets

more ^{2}D outlets may be beneficial. This is illustrated in Fig. 3, which shows the mass-weighted average velocities through the different ^{2}D outlets for devices with 5, 9 and 17 ^{2}D channels. Clearly, in a device with many channels nearly equal velocities can be obtained in all ^{2}D channels, except the extreme ones. The locations of the inversion points will affect the fractionation of an eventual spatial separation obtained in the ^{1}D channels across the various ^{2}D channels. Variations in the locations in comparison with the design values will lead to a distortion of the horizontal axis of the ^{1}D separation. Any velocity deviations between the various ^{2}D channels will influence the final ^{2}D separations. In principle, these later variation can be corrected for if every channel is monitored independently and a suitable t_0 marker or internal stand is present in the chromatograms. Both types of variations will be reduced in devices with greater numbers of outlets, as shown in Fig. 3. In our CFD simulations all channels of the FD were exactly equal and no (monolithic) frits were assumed to be present. Also, all ^{2}D channels were assumed equal in length. The creation of frits or stationary phases in a real device may reduce variations in flow rates between different channels.

Experimental Results

A five-outlet device was fabricated by 3D printing to study the flow profiles and the velocities in the 3D-printed devices. The experimentally obtained distribution ratios for the nine-outlet and five-outlet devices were compared with the results of CFD simulations (see Fig. 4). In both devices, there was a significant variation between the experimental and the simulated profiles. This may be caused by the experimental setup, for example by differences in the backpressure induced by variations in the PEEK tubing, the presence of small air bubbles, or by printing imperfections. The different percentages observed per outlet reflect the flow rates within the channel segments. In the eventual operation of the device,
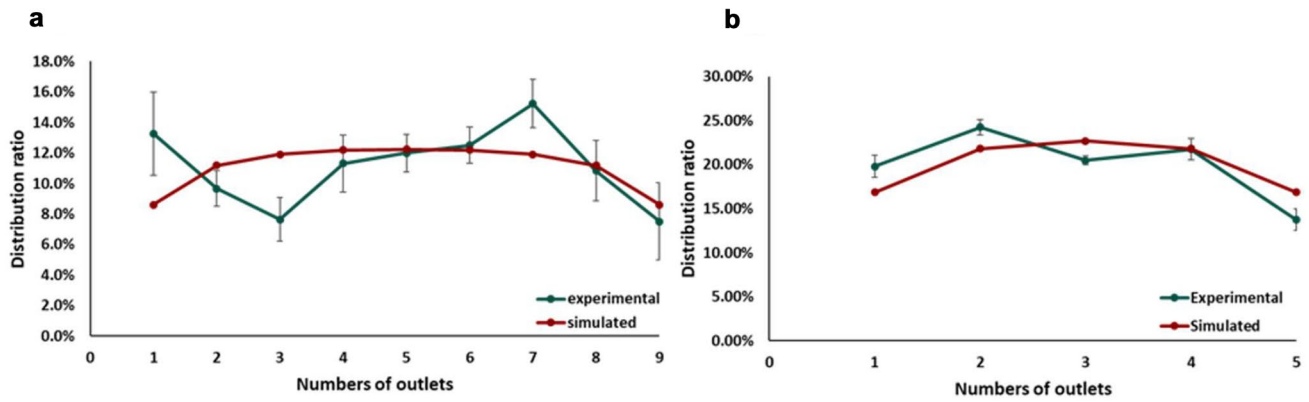
Fig. 4 Comparison of the distribution ratios between CFD simulations (red) and from experiments (green), **a** nine-outlet device and **b** five-outlet device

more-equal flow rates may be obtained in the different channels due to the presence of a stationary phase and the resulting higher backpressures. In principle, variations in channel flow rates can be dealt with by correcting time scales using marker compounds.

Peak-Width Evaluation

To investigate the sample transfer from the ^{1}D separation to the ^{2}D separation, transient CFD simulations were performed with tracer injections (see "Transient simulations"). To reduce the computational time, only one segment was selected for the simulation (centre outlet of the device, outlined in orange, see Fig. 5a). The species (ten proteins) were

equally spaced in the segment close to the centre of the outlet at the beginning of the simulation (see inlet in Fig. 5a). Subsequently, the species were flushed to the outlet and the data were collected at a distance of 5 mm from the ^{1}D channel (see arrow). The data were used to calculate the first and second moments. Figure 5b shows the first moment (left axis) and second moment (right axis) plotted against the initial distance (x) from the central outlet. The difference between the first protein and the last protein is approximately 11 s, indicating a flow velocity in the selected ^{1}D segment of $6.8/11 \approx 0.6$ mm s^{-1}.

It seems that both the migration time (μ_1) and the variance (μ_2) increase with the distance travelled, as expected. Also the second moment increases with the peak width obtained
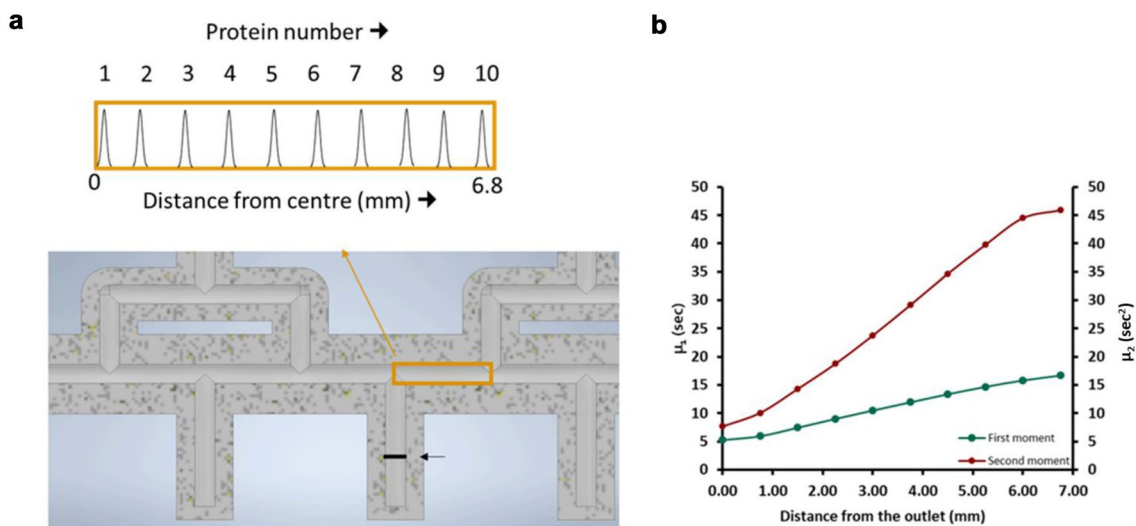

Fig. 5 Obtained results of investigation of the sample transfer from the ^{1}D separation to the ^{2}D separation. **a** Transient CFD simulations assuming ten equally distanced protein peaks (as indicated in the insert) being transferred from the ^{1}D channel. Drawn lines between

points are for visualization only. **b** Moments plotted against the initial distance (x) from the central outlet, first (left-hand axis) and second (right-hand axis) moments, 5 mm into the ^{2}D channel (black arrow)

in the first dimension (see Supplementary Material Fig. S1). The first and last points may deviate from the general trend, because initially they are positioned exactly at the centre of the outlet channel. Peaks #1 and #10 imply that half of it enters the outlet channel from either side, causing its variance to be reduced.

The peak width of a focused protein is different for each protein and is dependent on the diffusion coefficient of the protein and the voltage applied during the isoelectric focusing in the first dimension. Since the applied voltage is constant for all proteins that are being focused, only the diffusion coefficient of the protein is a variable. Variation in the diffusion coefficient will lead to different peak widths of the focused proteins. Different peak widths within a segment could cause different second moments, but this is not a big issue during flushing. The first and last points may deviate from the general trend, because initially they are positioned exactly at the centre of the outlet channel. For peak #1, this implies that half of the peak enters the outlet channel from either side. For peak #10, this implies that only half the peak is flushed to the considered outlet, causing its variance to be reduced. Proteins that are focused in the vicinity of an inlet will split up across two outlets, in varying ratios, as illustrated in Fig. 6. The ratio of the split is seen to depend on the location of the peak top relative to the centre of the inlet channel and on the peak width after the ^{1}D separation (standard deviation, 1 s).

The transfer from the first to the second dimension is seen to be efficient, but the position of the peak after the ^{1}D separation is not defined, because the centre outlet is fed from both the right and the left. Peaks positioned at equal distances to the left and right of the axis are flushed out simultaneously. This indicates the limited separation power of a channel with just five outlets. The useful peak capacity of the first-dimension separation cannot exceed five. To
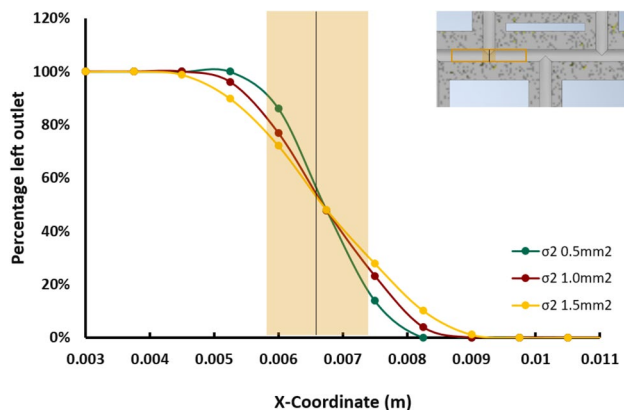
achieve high separation powers (high 2D peak capacities), many ^{2}D channels or a continuous (packed or monolithic) ^{2}D separation bed would be required. What the calculations reveal is that the transfer mechanism in sufficiently efficient to function correctly with many more ^{2}D channels.

Effect of Flow Confinement

A major challenge to reach the potential of spatial 2D-LC is to achieve adequate flow control and confinement of the analytes to the desired regions. Specifically, during the ^{1}D separation the mobile-phase flow and the analytes therein must be confined to the ^{1}D channel. For the present configuration, we have investigated whether and how a well-defined injection of a mixture into the ^{1}D channel will result in the migration of analytes into the flow distributor channels. If the connections between the ^{1}D channel and the flow distributor are open, ampholytes will enter the flow distributor and the pH gradient (with the same form in the direction of the ^{1}D channel) is also formed in the flow distributor during an IEF measurements. Analyte proteins may then also be distributed in channels of the flow distributor during IEF. This will result in peak deformation and potentially split peaks ("duplets") upon transfer to the ^{2}D channels. Different proteins with different pIs will distribute differently and—potentially—give rise to very different peak shapes.

To test whether the flow confinement in the ^{1}D channel is adequate, the tracer profile for a single analyte can be studied with CFD simulations. The effects of a poorly contained ^{1}D channel were studied by randomly positioning seven tracers in the channels and comparing the resulting profiles in five different outlets.

In Fig. 7, exemplary results are depicted for tracer 2 and tracer 6 for simulations of the ^{1}D channel without any confinement measures in place. The profiles of the tracers can be seen in Supplementary Material (Figure S2). In Fig. 7a, the tracer profile of tracer 2 is shown (see insert for the position in the ^{1}D channel), and it can be observed that the profile from outlet 2 shows a split peak emerging from the second ^{2}D outlet. One maximum arises from the analyte band positioned in the ^{1}D channel; the second maximum arises from the second analyte band focused in the flow distributor (see insert in Fig. 7). Similar behaviour is seen in tracer 6 from outlet 3 (see Fig. 7b). Tracer profiles with duplets or triplets can have implications for eventual ^{1}D and ^{2}D separations. For ^{2}D separation, the ^{2}D mobile phase has to flow through the flow distributor and flush the analytes into the ^{2}D regions. The same analyte appearing in different outlets will severely limit the separation power of the ^{1}D step. For ^{1}D spatial fractionation this can potentially be overcome by stopping the flushing of analytes before the later peaks reach the outlets. However, this may lead to analyte loss and reduced recovery.
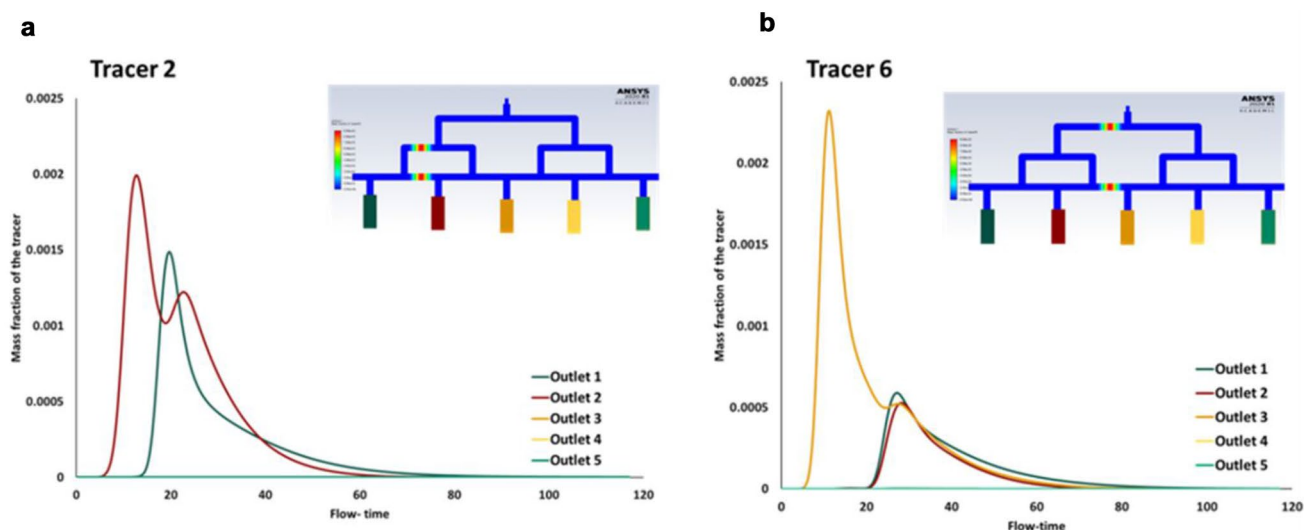

Fig. 6 Split ratios for peaks located in the vicinity of inlet channels for different peak widths after the ^{1}D separation. Feak widths in terms of four times the standard deviation $4 \times {}^1\sigma$ equal to 2.82 mm (green line), 4.00 mm (dark red), and 4.90 mm (dark yellow)

Fig. 7 Simulated band profiles resulting from tracer pulses located in different positions within the flow distributor at $t=0$

Conclusion

Several aspects of prospective spatial 2D-LC systems were studied, viz. efficient transfer of samples between the two dimensions and the flow behaviour within the device. The flow behaviour within a device will also influence the sample transfer between the two dimensions. Focus was on the computational transient and steady-state simulations to study flow velocity and band broadening. For a five-outlet device, it was found that the total flow was not equally divided across the outlets of the flow distributor and that the magnitude of the flow was not equal in each segment of the ^{1}D channel. The segment at the extremes showed higher velocities compared to the central parts of the channel. Any velocity deviations between the various ^{2}D channels will influence the final ^{2}D separations. Based on transient CFD simulations with tracer injections, it was concluded that the migration times (first moment, μ_1) and the variances (second moment, μ_2) increase with the distance travelled, as expected. Also, the location of the eventually focused proteins is of importance. It was observed that proteins that are focused in the vicinity of an inlet will split up across two outlets in varying ratios. Such effects can be reduced by increasing the number of channels or, eventually, using a continuous packed bed or monolithic stationary phase in the second dimension. The present study has contributed to progress in spatial 2D-LC separations. The understanding of the effects of the location of peaks in the device gained from the present study should contribute to the realization of successful ^{2}D separations.

Declarations

References

1. Pirok BWJ, Gargano AFG, Schoenmakers PJ (2018) Optimizing separations in online comprehensive two-dimensional liquid chromatography. J Sep Sci 41:68–98. https://doi.org/10.1002/jssc.201700863
2. Pirok BWJ, Stoll DR, Schoenmakers PJ (2019) Recent developments in two-dimensional liquid chromatography: fundamental

improvements for practical applications. Anal Chem 91:240–263. https://doi.org/10.1021/acs.analchem.8b04841

3. Ramsey JD, Jacobson SC, Culbertson CT, Ramsey JM (2008) High-efficiency, two-dimensional separations of protein digests on microfluidic devices. Anal Chem 75:3758–3764

4. Davydova E, Wouters S, Deridder S et al (2016) Design and evaluation of microfluidic devices for two-dimensional spatial separations. J Chromatogr A 1434:127–135. https://doi.org/10.1016/j.chroma.2016.01.003

5. Liu J, Yang S, Lee CS, DeVoe DL (2008) Polyacrylamide gel plugs enabling 2-D microfluidic protein separations via isoelectric focusing and multiplexed sodium dodecyl sulfate gel electrophoresis. Electrophoresis 29:2241–2250. https://doi.org/10.1002/elps.200700608

6. Rocklin RD, Ramsey RS, Ramsey JM (2000) A microfabricated fluidic device for performing two-dimensional liquid-phase separations. Anal Chem 72:5244–5249. https://doi.org/10.1021/ac000578r

7. Abdulhussain N, Nawada S, Schoenmakers P (2021) Latest trends on the future of three-dimensional separations in chromatography. Chem Rev. https://doi.org/10.1021/acs.chemrev.0c01244

8. Themelis T, Amini A, De Vos J, Eeltink S (2021) Towards spatial comprehensive three-dimensional liquid chromatography: A tutorial review. Anal Chim Acta. https://doi.org/10.1016/j.aca.2020.12.032

9. Yang S, Liu J, Lee S, Devoe DL (2009) Microfluidic 2-D PAGE using multifunctional in situ polyacrylamide gels and discontinuous buffers. Lab Chip. https://doi.org/10.1039/b805541f

10. Wouters B, de Vos J, Desmet G, Terryn H, Schoenmakers PJ, Eeltink S (2015) Design of a microfluidic device for comprehensive spatial two-dimensional liquid chromatography. J Sep Sci 38(7):1123–1129

11. Adamopoulou T, Nawada S, Deridder S et al (2019) Experimental and numerical study of band-broadening effects associated with analyte transfer in microfluidic devices for spatial two-dimensional liquid chromatography created by additive manufacturing. J Chromatogr A 1598:77–84. https://doi.org/10.1016/j.chroma.2019.03.041

12. van Oss CJ (1977) A Review of: "Isoelectric Focusing, N. Catsimpoolas, Ed. Academic Press, New York, 1976; hardbound, 265 pages, $23.50." Prep Biochem 7:303. https://doi.org/10.1080/00327487708061646

13. Silvertand LHH, Toraño JS, van Bennekom WP, de Jong GJ (2008) Recent developments in capillary isoelectric focusing. J Chromatogr A 1204:157–170. https://doi.org/10.1016/j.chroma.2008.05.057

14. Emrich CA, Medintz IL, Chu WK, Mathies RA (2007) Microfabricated two-dimensional electrophoresis device for differential protein expression profiling. Anal Chem 79:7360–7366. https://doi.org/10.1021/ac0711485

15. Yang S, Liu J, Devoe DL (2008) Optimization of sample transfer in two-dimensional microfluidic separation systems. Lab Chip. https://doi.org/10.1039/b801978a

16. Hirsch C (2007) Introduction: an initial guide to CFD and to this volume. In: Hirsch CBT-NC of I and EF (Second E (ed). Butterworth-Heinemann, Oxford, pp 1–V